Crystal Structures of the Soluble Methane Monooxygenase Hydroxylase from *Methylococcus capsulatus* (Bath) Demonstrating Geometrical Variability at the Dinuclear Iron Active Site

Douglas A. Whittington and Stephen J. Lippard*

Contribution from the Department of Chemistry, Massachusetts Institute of Technology, Cambridge, Massachusetts 02139

Received August 31, 2000

Abstract: The oxidation of methane to methanol is performed at carboxylate-bridged dinuclear iron centers in the soluble methane monooxygenase hydroxylase (MMOH). Previous structural studies of MMOH, and the related R2 subunit of ribonucleotide reductase, have demonstrated the occurrence of carboxylate shifts involving glutamate residues that ligate the catalytic iron atoms. These shifts are thought to have important mechanistic implications. Recent kinetic and theoretical studies have also emphasized the importance of hydrogen bonding and pH effects at the active site. We report here crystal structures of MMOH from *Methylococcus capsulatus* (Bath) in the diiron(II), diiron(III), and mixed-valent Fe(II)Fe(III) oxidation states, and at pH values of 6.2, 7.0, and 8.5. These structures were investigated in an effort to delineate the range of possible motions at the MMOH active site and to identify hydrogen-bonding interactions that may be important in understanding catalysis by the enzyme. Our results present the first view of the diiron center in the mixed-valent state, and they indicate an increased lability for ferrous ions in the enzyme. Alternate conformations of Asn214 near the active site according to redox state and a distortion in one of the α-helices adjacent to the metal center in the diiron(II) state have also been identified. These changes alter the surface of the protein in the vicinity of the catalytic core and may have implications for small-molecule accessibility to the active site and for protein component interactions in the methane monooxygenase system. Collectively, these results help to explain previous spectroscopic observations and provide new insight into catalysis by the enzyme.

Introduction

Proteins containing carboxylate-bridged dinuclear iron centers are members of a select class of metalloenzymes capable of activating dioxygen for subsequent oxidation chemistry. The best-studied members of this group of enzymes are the soluble methane monooxygenase hydroxylase (MMOH), which oxidizes methane to methanol, the R2 subunit of class I ribonucleotide reductases (RNR-R2), which generates a tyrosyl radical essential for the reduction of ribonucleotides to deoxyribonucleotides in DNA biosynthesis, and the stearoyl acyl carrier protein Δ-9 desaturase (Δ9-ACP), which introduces a double bond into saturated fatty acids.[1−3] Whereas the chemistry performed by these enzymes and their overall structures differ markedly, their active sites are strikingly similar.[4,5] Each diiron center is located in a 4-helix bundle of α-helices (Figure 1) contained within a larger protein structure. Ligands are provided by the 2-fold repeat of a motif containing a single aspartic or glutamic acid on one helix followed by a glutamic acid and a histidine arranged in an E−X−X−H sequence on the neighboring helix. The remainder of the coordination sphere is filled by solvent-derived oxo, hydroxo, or aqua ligands. This structural assembly has been nicely reduced to a minimalist set of key relations in work by DeGrado and co-workers.[6]

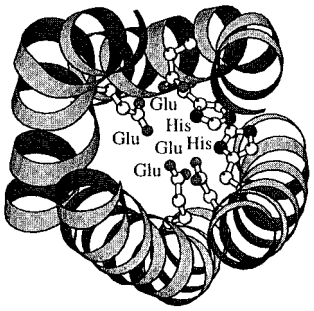

Figure 1. Four-helix bundle containing two repeats of a D/E···EXXH amino acid motif that serve as ligands for dinuclear iron active sites.

The oxygen-rich coordination environment in MMOH, as well as in RNR-R2 and Δ9-ACP, is thought to be important for the formation of high-valent iron intermediates in the catalytic cycle of these enzymes. Spectroscopic evidence exists for the formation of a diiron(IV) intermediate in MMOH,[7−11] and an Fe(III)Fe(IV) intermediate has been demonstrated in RNR-R2.[12] Δ9-ACP may also form a high-valent intermediate in its catalytic

(1) Feig, A. L.; Lippard, S. J. *Chem. Rev.* **1994**, *94*, 759−805.
(2) Wallar, B. J.; Lipscomb, J. D. *Chem. Rev.* **1996**, *96*, 2625−2657.
(3) Solomon, E. I.; Brunold, T. C.; Davis, M. I.; Kemsley, J. N.; Lee, S.-K.; Lehnert, N.; Neese, F.; Skulan, A. J.; Yang, Y.-S.; Zhou, J. *Chem. Rev.* **2000**, *100*, 235−349.
(4) Nordlund, P.; Eklund, H. *Curr. Opin. Struct. Biol.* **1995**, *5*, 758−766.
(5) Kurtz, D. M., Jr. *J. Biol. Inorg. Chem.* **1997**, *2*, 159−167.
(6) Lombardi, A.; Summa, C. M.; Geremia, S.; Randaccio, L.; Pavone, V.; DeGrado, W. F. *Proc. Natl. Acad. Sci. U.S.A.* **2000**, *97*, 6298−6305.
(7) Lee, S.-K.; Nesheim, J. C.; Lipscomb, J. D. *J. Biol. Chem.* **1993**, *268*, 21569−21577.
(8) Lee, S.-K.; Fox, B. G.; Froland, W. A.; Lipscomb, J. D.; Münck, E. *J. Am. Chem. Soc.* **1993**, *115*, 6450−6451.
(9) Liu, K. E.; Wang, D.; Huynh, B. H.; Edmondson, D. E.; Salifoglou, A.; Lippard, S. J. *J. Am. Chem. Soc.* **1994**, *116*, 7465−7466.
(10) Liu, K. E.; Valentine, A. M.; Wang, D.; Huynh, B. H.; Edmondson, D. E.; Salifoglou, A.; Lippard, S. J. *J. Am. Chem. Soc.* **1995**, *117*, 10174−10185.

10.1021/ja003240n CCC: $20.00
Published on Web 01/12/2001

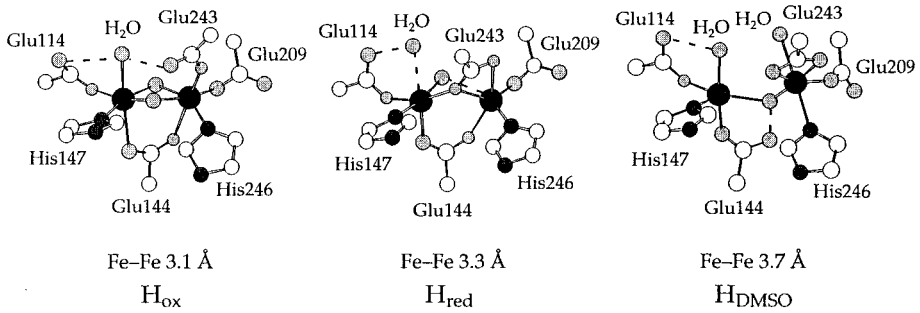

Figure 2. Dinuclear iron active sites in *M. capsulatus* (Bath) MMOH from previously published structures (see refs 32 and 33). Amino acid ligands are labeled and the Fe−Fe separations are given. The carboxylate shifts in Glu243 are apparent.

cycle.[13] Moreover, spectroscopic results indicate that there are many similarities between the reaction cycle intermediates of these enzymes. For example, the diiron(II) forms of MMOH, Δ9-ACP, and D84E RNR-R2 react with dioxygen to form diiron(III) peroxo intermediates that display very similar Mössbauer parameters.[9,10,14,15] In addition, the diiron(IV) intermediate Q in MMOH can be reduced by one electron at 77 K to yield an Fe(III)Fe(IV) species that closely resembles the Fe(III)Fe(IV) intermediate X of RNR-R2.[16] Despite these similarities, there are chemical differences among the systems, and a major goal in this field is to determine how the protein controls reactivity at the active site.

In the soluble methane monooxygenase system (sMMO) from the methanotrophic bacterium *Methylococcus capsulatus* (Bath), MMOH acts in concert with two other proteins, a reductase (MMOR) and a coupling protein (MMOB), to catalyze the oxidation of methane to methanol. MMOH is a large, 251-kDa protein that exists as an $\alpha_2\beta_2\gamma_2$ homodimer. The catalytically active, carboxylate-bridged dinuclear iron centers are housed in the α subunits. The reductase uses its FAD and Fe_2S_2 cofactors to shuttle electrons from NADH to the dinuclear iron active site.[17,18] MMOB alters reduction potentials at the diiron center, aids in substrate access to the active site, and couples the system to perform monooxygenase chemistry.[19−26] Efficient catalysis requires all three components.

The structures of MMOH and MMOB are known for both the *M. capsulatus* (Bath) system[27,28] and the other well-studied system from *Methylosinus trichosporium* OB3b.[29,30] Each MMOH structure has been solved in two crystal forms,[29,31] and crystals of one form of MMOH from the *M. capsulatus* (Bath) system have been investigated in both the oxidized and reduced states.[32] A third variation of the *M. capsulatus* (Bath) MMOH structure was observed in crystals soaked in a 10% DMSO solution prior to data collection.[33] A comparison of the dinuclear iron active sites in all of the known structures from the two organisms reveals alternate orientations for several side chains at the active site, including Leu110, Asn214, and Glu243, which serves as a ligand to iron (Figure 2).[34] A range of Fe−Fe separations from 3.0 to 3.7 Å is also apparent.

The shifts observed in the conformation of Glu243 are illustrative of a concept known as the carboxylate shift, a phenomenon that takes advantage of the multiple possibilities for carboxylate ligation to dimetallic centers.[35] Carboxylate shifts in the active site of MMOH are thought to be important in controlling the number of open coordination sites and in accommodating a range of Fe−Fe distances during catalysis. Similar carboxylate shifts have also been observed in the RNR-R2 active site when comparing oxidized and reduced structures of the native and D84E mutants[36] and in the reduced, azide-bound F208A/Y122F mutant.[37] Recent density functional theory (DFT) calculations on the MMOH active site also support the conclusion that carboxylate shifts are important for catalysis.[38] In addition, the DFT calculations emphasize the role of the carboxylate oxygen atoms in forming important hydrogen bonds to mediate close oxygen−oxygen contacts in the oxygen-rich

(11) Shu, L.; Nesheim, J. C.; Kauffmann, K.; Münck, E.; Lipscomb, J. D.; Que, L., Jr. *Science* **1997**, *275*, 515−518.
(12) Bollinger, J. M., Jr.; Edmondson, D. E.; Huynh, B. H.; Filley, J.; Norton, J. R.; Stubbe, J. *Science* **1991**, *253*, 292−298.
(13) Broadwater, J. A.; Laundre, B. J.; Fox, B. G. *J. Inorg. Biochem.* **2000**, *78*, 7−14.
(14) Moënne-Loccoz, P.; Baldwin, J.; Ley, B. A.; Loehr, T. M.; Bollinger, J. M., Jr. *Biochemistry* **1998**, *37*, 14659−14663.
(15) Broadwater, J. A.; Achim, C.; Münck, E.; Fox, B. G. *Biochemistry* **1999**, *38*, 12197−12204.
(16) Valentine, A. M.; Tavares, P.; Pereira, A. S.; Davydov, R.; Krebs, C.; Hoffman, B. M.; Edmondson, D. E.; Huynh, B. H.; Lippard, S. J. *J. Am. Chem. Soc.* **1998**, *120*, 2190−2191.
(17) Lund, J.; Dalton, H. *Eur. J. Biochem.* **1985**, *147*, 291−296.
(18) Lund, J.; Woodland, M. P.; Dalton, H. *Eur. J. Biochem.* **1985**, *147*, 297−305.
(19) Paulsen, K. E.; Liu, Y.; Fox, B. G.; Lipscomb, J. D.; Münck, E.; Stankovich, M. T. *Biochemistry* **1994**, *33*, 713−722.
(20) Liu, K. E.; Lippard, S. J. *J. Biol. Chem.* **1991**, *266*, 12836−12839, 24859.
(21) Liu, Y.; Nesheim, J. C.; Lee, S.-K.; Lipscomb, J. D. *J. Biol. Chem.* **1995**, *270*, 24662−24665.
(22) Davydov, R.; Valentine, A. M.; Komar-Panicucci, S.; Hoffman, B. M.; Lippard, S. J. *Biochemistry* **1999**, *38*, 4188−4197.
(23) Pulver, S. C.; Froland, W. A.; Lipscomb, J. D.; Solomon, E. I. *J. Am. Chem. Soc.* **1997**, *119*, 387−395.
(24) Green, J.; Dalton, H. *J. Biol. Chem.* **1985**, *260*, 15795−15801.
(25) Kazlauskaite, J.; Hill, H. A. O.; Wilkins, P. C.; Dalton, H. *Eur. J. Biochem.* **1996**, *241*, 552−556.
(26) Gassner, G. T.; Lippard, S. J. *Biochemistry* **1999**, *38*, 12768−12785.
(27) Rosenzweig, A. C.; Frederick, C. A.; Lippard, S. J.; Nordlund, P. *Nature* **1993**, *366*, 537−543.
(28) Walters, K. J.; Gassner, G. T.; Lippard, S. J.; Wagner, G. *Proc. Natl. Acad. Sci. U.S.A.* **1999**, *96*, 7877−7882.
(29) Elango, N.; Radhakrishnan, R.; Froland, W. A.; Wallar, B. J.; Earhart, C. A.; Lipscomb, J. D.; Ohlendorf, D. H. *Protein Sci.* **1997**, *6*, 556−568.
(30) Chang, S.-L.; Wallar, B. J.; Lipscomb, J. D.; Mayo, K. H. *Biochemistry* **1999**, *38*, 5799−5812.
(31) Rosenzweig, A. C.; Brandstetter, H.; Whittington, D. A.; Nordlund, P.; Lippard, S. J.; Frederick, C. A. *Proteins* **1997**, *29*, 141−152.
(32) Rosenzweig, A. C.; Nordlund, P.; Takahara, P. M.; Frederick, C. A.; Lippard, S. J. *Chem. Biol.* **1995**, *2*, 409−418.
(33) Rosenzweig, A. C.; Frederick, C. A.; Lippard, S. J. In *Microbial Growth on C1 Compounds*; Lidstrom, M. E., Tabita, F. R., Eds.; Kluwer Academic Publishers: Boston, 1996; pp 141−149.
(34) Whittington, D. A.; Lippard, S. J. In *Spectroscopic Methods in Bioinorganic Chemistry*; Solomon, E. I., Hodgson, K. O., Eds.; American Chemical Society: Washington, DC, 1998; pp 334−347.
(35) Rardin, R. L.; Tolman, W. B.; Lippard, S. J. *New J. Chem.* **1991**, *15*, 417−430.
(36) Voegtli, W. C.; Khidekel, N.; Baldwin, J.; Ley, B. A.; Bollinger, J. M., Jr.; Rosenzweig, A. C. *J. Am. Chem. Soc.* **2000**, *122*, 3255−3261.
(37) Andersson, M. E.; Högbom, M.; Rinaldo-Matthis, A.; Andersson, K. K.; Sjöberg, B.-M.; Nordlund, P. *J. Am. Chem. Soc.* **1999**, *121*, 2346−2352.
(38) Dunietz, B. D.; Beachy, M. D.; Cao, Y.; Whittington, D. A.; Lippard, S. J.; Friesner, R. A. *J. Am. Chem. Soc.* **2000**, *122*, 2828−2839.

coordination sphere of MMOH and, by implication, related diiron enzymes. Since all of the reactions catalyzed by this family of enzymes require the efficient handling of protons, identification of the means by which they do so is of considerable importance. Experimental results from pH studies of the MMOH reaction illustrate the sensitivity of the reactions to the availability of protons.[39]

In an effort to define further the range of motions possible for glutamate ligands at the MMOH active site, to delineate the positions of important hydrogen-bonding partners, and to gain insight into how the protein structure promotes C−H bond activation in this enzyme, we determined crystal structures of crystal form II MMOH in the oxidized (H_{ox}), mixed-valent (H_{mv}), and reduced (H_{red}) states, as well as at pH values of 6.2, 7.0, and 8.5. The mixed-valent Fe(II)Fe(III) and reduced Fe(II)Fe(II) forms were prepared both by soaking oxidized crystals in the appropriate mediator solutions as well as by growing crystals of MMOH under anaerobic conditions. The results provide novel views of the active-site structure and allow us to identify additional hydrogen-bonding interactions that may be important during catalysis. The new findings are interpreted in light of previous spectroscopic results with MMOH, and in comparison to other diiron-containing enzymes.

Experimental Section

Protein Isolation and Purification. MMOH was isolated from *M. capsulatus* (Bath) cells grown by fermentation in 15 L batches, and purified as described previously.[40,41] Protein purity was established by denaturing polyacrylamide gel electrophoresis. Purified MMOH was exchanged into 25 mM *N*-morpholinopropane sulfonic acid (MOPS), pH 7.0, containing 5% (v/v) glycerol and concentrated to ≥50 μM (Centriprep or Centricon, Amicon) for subsequent use in crystallization trials. The specific activity and iron content of MMOH were in the ranges described previously.[26,42,43]

Protein Crystallization. MMOH crystals in space group $P2_12_12_1$ having unit cell dimensions $a = 72$ Å, $b = 172$ Å, and $c = 222$ Å were grown at room temperature by a modification of the published conditions.[31] The asymmetric unit houses one complete MMOH dimer. The well solutions of the hanging drop crystallization trays contained 6% (w/w) poly(ethylene glycol) (PEG) 8000, 50 mM MOPS, pH 7.0, 200 mM $CaCl_2$, and 0.01% sodium azide. Drops consisted of 3 μL of 50 mM MMOH, 1.5 μL of 50%-saturated 1,10-decanedioic acid (in H_2O), and 1.5 μL of 12% PEG 8000, 100 mM MOPS, pH 7.0, 440 mM $CaCl_2$ and 0.02% sodium azide. To ensure the formation of large, single crystals suitable for data collection, the drops were microseeded after 2 days. Microseed stock was prepared by harvesting all of the crystals out of one drop from a previous plate into a stabilizing buffer consisting of 10% PEG 8000, 50 mM MOPS, pH 7.0, and 220 mM $CaCl_2$. The crystals were washed by successive transfer into three 500 μL volumes of the stabilizing buffer and then crushed in 1.0 mL of stabilizing buffer in a 2.0 mL glass homogenizer. A 10^{-3} dilution of this "seed stock" was made, and 0.7 μL of this solution was used to seed the new trays. Large, single crystals (0.3 × 0.3 × 0.4 mm) suitable for data collection appeared in 4−7 days.

MMOH in the mixed-valent Fe(II)Fe(III) and reduced diiron(II) states was crystallized by using the same conditions in a 4 °C anaerobic chamber (Coy). To prepare mixed-valent MMOH, a 155 μL sample of 200 μM protein was made anaerobic by ∼15 cycles of vacuum evacuation followed by back-filling with argon. This solution contained the mediators phenazine methosulfate, methylene blue, and potassium indigotetrasulfonate at a 200 μM concentration, and the protein was reduced by addition of dithionite as described previously.[44] The sample was equilibrated for 45 min at 4 °C and then brought into the anaerobic chamber where the dithionite and mediators were removed by dialysis in deaerated 25 mM MOPS, pH 7.0, buffer. Reduced MMOH was prepared in a similar fashion, except that a stoichiometric amount of methyl viologen was used in place of the other mediators. The methyl viologen and dithionite were similarly removed by dialysis under anaerobic conditions. Stock solutions of 30% PEG 8000 and 2.0 M $CaCl_2$ for use in crystallization trials were made anaerobic by placing a weighed quantity of the solid compound in a glass bottle, which was then sealed with a rubber septum. The air was removed by repeated vacuum and back-filling with argon. An appropriate amount of degassed, distilled, deionized water (Millipore) was then added to these samples in the anaerobic chamber to create the stock solution. The 1.0 M MOPS, pH 7.0, stock solution was made in air and degassed with H_2O-saturated argon.

Crystal Soaking. Oxidized crystals were brought into the anaerobic chamber and placed in 500 μL of a cryosolution (25% glycerol, 10% PEG 8000, 50 mM MOPS, pH 7.0, 200 mM $CaCl_2$) containing 200 μM phenazine methosulfate, methylene blue, and potassium indigotetrasulfonate. The mediators were reduced by addition of 4 μL of ∼0.5 M dithionite, and crystals were soaked in this solution to convert them to the mixed-valent state. They were then packed in capillary tubes with excess solution, sealed, and transported to the Stanford Synchrotron Radiation Laboratory (SSRL). To mount the crystals, the capillaries were opened, and the crystals were quickly transferred to rayon loops and flash-frozen in the nitrogen stream at −165 °C. The cryosolution used for transporting and mounting the crystals contained the mediators to ensure that the protein stayed in the desired redox state and did not oxidize back to the diiron(III) form. The solution maintained a yellow color throughout transport and mounting, indicating that it did not reoxidize. The total soaking time was 19 h. The preparation of reduced crystals by soaking followed a similar protocol, except that the cryosolution contained 200 μM of methyl viologen reduced by addition of 4 μL of ∼0.5 M dithionite. The crystals were soaked for 1 h in this solution and then flash-frozen in a cold nitrogen stream at MIT. The frozen crystals were shipped to the Structural Biology Center (SBC) at the Advanced Photon Source at Argonne National Laboratories.

The redox states of the crystals were assigned on the basis of the known behavior of MMOH treated with solutions of dithionite and the mediators listed above. All of the crystal manipulations for reduced states of the enzyme were performed under anaerobic conditions, and the soaking experiments contained mediators, the visible colors of which could be used to verify the reduced nature of the solution. An attempt to obtain a single crystal EPR spectrum of the mixed-valent crystals was not successful. Combinations of X-ray absorption spectroscopic and X-ray diffraction experiments are planned as an independent measure of oxidation state. The observed active site structural rearrangements (see Results), especially those of the reduced state which are analogous to previous structural results with MMOH and with mutants of RNR-R2, argue in favor of the assigned redox state changes.

To investigate the effects of pH, oxidized crystals were harvested and transferred into 500 μL of a stabilizing solution containing either 0.1 M PIPES, pH 6.2, or 0.1 M Tris, pH 8.5, in place of MOPS, pH 7.0. After soaking overnight, the crystals were then mounted and flash-frozen in the cold nitrogen stream.

Data Collection. Diffraction data were collected either at SSRL on beamline 9-1, or on beamline 19-ID of the SBC at the Advanced Photon Source of Argonne National Laboratories. At SSRL, diffraction data were collected at −165 °C and recorded on a Mar 345 imaging plate detector. The diffraction data from the SBC were collected on an Electronic Computing Technologies 3 × 3 CCD detector from crystals frozen at 100 K. All data were indexed and scaled using the HKL suite of programs.[45] Data collection statistics appear in Table 1.

(39) Lee, S.-K.; Lipscomb, J. D. *Biochemistry* **1999**, *38*, 4423−4432.
(40) DeWitt, J. G.; Bentsen, J. G.; Rosenzweig, A. C.; Hedman, B.; Green, J.; Pilkington, S.; Papaefthymiou, G. C.; Dalton, H.; Hodgson, K. O.; Lippard, S. J. *J. Am. Chem. Soc.* **1991**, *113*, 9219−9235.
(41) Willems, J.-P.; Valentine, A. M.; Gurbiel, R.; Lippard, S. J.; Hoffman, B. M. *J. Am. Chem. Soc.* **1998**, *120*, 9410−9416.
(42) Valentine, A. M.; LeTadic-Biadatti, M.-H.; Toy, P. H.; Newcomb, M.; Lippard, S. J. *J. Biol. Chem.* **1999**, *274*, 10771−10776.
(43) Coufal, D. E.; Tavares, P.; Pereira, A. S.; Hyunh, B. H.; Lippard, S. J. *Biochemistry* **1999**, *38*, 4504−4513.
(44) DeRose, V. J.; Liu, K. E.; Kurtz, D. M., Jr.; Hoffman, B. M.; Lippard, S. J. *J. Am. Chem. Soc.* **1993**, *115*, 6440−6441.
(45) Otwinowski, Z.; Minor, W. *Methods Enzymol.* **1997**, *276*, 307−326.

Table 1. Data Collection Statistics

	H_{ox}	H_{mv}-soak	H_{mv}-grown	H_{red}-soak	H_{red}-grown	$H_{pH6.2}$	$H_{pH8.5}$
X-ray source	SSRL	SSRL	SSRL	SBC/APS	SSRL	SSRL	SSRL
wavelength (Å)	0.980	0.970	1.08	1.033	0.980	0.980	1.08
temperture (K)	98	108	98	100	93	98	98
space group	$P2_12_12_1$	$P2_12_12_1$	$P2_12_12_1$	$P2_12_12_1$	$P2_12_12_1$	$P2_12_12_1$	$P2_12_12_1$
cell dimensions[a]							
a (Å)	71.4	71.4	71.4	71.3	71.2	71.4	70.9
b (Å)	172.0	171.9	171.7	171.7	171.6	172.1	171.5
c (Å)	221.4	221.5	221.5	221.6	220.5	221.4	221.7
resolution (Å)	30−1.96	30−2.15	50−2.07	30−2.15	50−2.40	30−2.03	30−2.38
total observations	1,641,424	1,442,213	1,736,424	2,132,118	907,358	1,834,988	820,337
unique reflections	194,787	148,446	165,782	145,320	104,366	175,589	103,150
R_{sym} (%)[b,c]	6.7 (36.2)	6.2 (36.0)	8.2 (45.1)	5.1 (24.1)	9.0 (47.0)	6.0 (34.9)	8.4 (50.3)
$I/\sigma(I)$[b]	17.3 (4.0)	19.3 (4.7)	13.7 (3.0)	21.3 (3.8)	12.5 (2.0)	18.9 (4.7)	11.6 (2.4)
completeness (%)[b]	99.5 (96.7)	99.8 (99.4)	99.5 (98.8)	98.1 (92.2)	97.9 (97.3)	99.5 (98.3)	91.5 (80.2)

[a] The asymmetric unit comprises one full MMOH dimer. [b] Values in parentheses are for the highest resolution shells. [c] $R_{sym} = \Sigma|I - \langle I\rangle|/\Sigma I$, where I is the observed intensity and $\langle I\rangle$ is the average intensity over all observations of symmetry-related reflections.

Table 2. Data Refinement Statistics

	H_{ox}	H_{mv}-soak	H_{mv}-grown	H_{red}-soak	H_{red}-grown	$H_{pH6.2}$	$H_{pH8.5}$
resolution range (Å)	30−1.96	30−2.15	30−2.07	30−2.15	30−2.40	30−2.03	30−2.38
no. reflections used	182,142	141,121	155,856	138,571	95,134	163,784	91,661
R_{cryst}[a]	0.200	0.192	0.193	0.189	0.218	0.196	0.223
R_{free}[b]	0.234	0.229	0.230	0.230	0.253	0.228	0.256
No. of protein atoms	17,502	17,497	17,509	17,509	17.478	17,511	17,494
No. of water molecules	1341	1161	1343	1232	527	1262	474
rms deviations							
bond lengths (Å)	0.005	0.005	0.005	0.006	0.007	0.005	0.007
bond angles (deg)	1.16	1.15	1.16	1.16	1.23	1.17	1.23
mean *B*-value (Å^2) (all atoms)	30.4	34.4	30.2	33.0	44.6	32.2	43.9
Luzzati coord. error (Å) (overall)	0.29	0.24	0.23	0.24	0.32	0.24	0.34
PDB code	1FZ1	1FZ2	1FZ0	1FYZ	1FZ5	1FZ3	1FZ4

[a] $R_{cryst} = \Sigma|F_{obs} - F_{calc}|/\Sigma F_{obs}$, where F_{obs} and F_{calc} are the observed and calculated structure factor amplitudes, respectively. [b] R_{free} was calculated from a randomly chosen subset of 3.5% of the reflections.

Data Refinement. Refinement of all structures was performed with CNS.[46] Manual rebuilding and structure manipulations were done in O.[47] Initial phases obtained from the oxidized MMOH crystal form II structure with all solvent removed were used as a starting model for rigid body refinement in CNS.[31] The R_{cryst} and R_{free} factors would typically drop to ~26% after this step. R_{free} was calculated from a test set of 3.5% of the reflections.[48] For refinements of mixed-valent and reduced MMOH, Glu243 was assigned as an Ala residue in the initial model to prevent bias in the positioning of its carboxylate side chain. Rigid body refinement was followed by grouped *B*-factor refinement. The models were then checked, and any necessary adjustments were made manually. Simulated-annealing refinements (3000 K) to remove previous model bias and individual *B*-factor refinements were then performed. After an additional manual inspection and rebuilding stage, the models were subjected to a round of positional and individual *B*-factor refinement followed by an automated peak-picking routine to locate putative water molecules. Only peaks ≥3.0 σ in the difference Fourier maps located between 2.5 and 3.3 Å from the protein backbone and having *B*-factors <60 Å^2 were written to a file. These peaks were then inspected manually in O, and any peaks not having corresponding electron density in the $|2|F_{obs}| - |F_{calc}||$ maps (1 σ contour) or lacking any obvious hydrogen-bonding partners were deleted. The models were subjected to additional cycles of positional and individual *B*-factor refinement followed by water picking in an iterative fashion. Typically 4−5 rounds were required to account for the water peaks. Once a complete model was obtained, a final round of refinements was run, and the active sites were examined. Simulated annealing difference omit maps were calculated, as necessary, to check features of electron density near the active sites. Throughout the refinements, the entire MMOH protein was refined as a single entity. Non-crystallographic symmetry (NCS) restraints were not applied in order to obtain two independent views of the dinuclear iron active sites, except in the case of the two lower-resolution structures, MMOH grown from reduced enzyme and MMOH soaked at pH 8.5. In these two structures, weak NCS restraints were applied between protomers during positional but not during *B*-factor refinement. The amino acids at the active site were not included in the NCS restraints. This refinement protocol resulted in cleaner electron density maps, a lower value of R_{free}, and a smaller separation between R and R_{free}. The accuracy of the protein model was assessed by using PROCHECK.[49] The calculated Luzzati coordinate errors for each structure and the refinement statistics appear in Table 2.

Results

Novel Aspects of the Overall Structure. In comparison to the previous structures of MMOH from *M. capsulatus* (Bath), the current series of structures has the same largely α-helical $\alpha_2\beta_2\gamma_2$ fold with overall dimensions of 60 × 100 × 120 Å (Figure 3). Additional amino acids at the termini of each subunit were identified, however, allowing the assignment of one additional key element of secondary structure. Residues Arg162 through Gln167 in the γ-subunits form a β-strand that interacts (in an antiparallel fashion) with residues Glu440 through Leu436 of the α-subunit to form a β-sheet. This secondary structural feature between subunits is the only one of its type, other than the numerous helix−helix packing interactions found throughout the protein. The complete β-subunit sequence and residues Asn17 through the C-terminal Asn527 of the α-subunit were

(46) Brünger, A. T.; Adams, P. D.; Clore, G. M.; DeLano, W. L.; Gros, P.; Grosse-Kunstleve, R. W.; Jiang, J.-S.; Kuszewski, J.; Nilges, M.; Pannu, N. S.; Read, R. J.; Rice, L. M.; Simonson, T.; Warren, G. L. *Acta Crystallogr. D* **1998**, *54*, 905−921.

(47) Jones, T. A.; Zou, J.-Y.; Cowan, S. W.; Kjeldgaard, M. *Acta Crystallogr. A* **1991**, *47*, 110−119.

(48) Brünger, A. T. *Nature* **1992**, *355*, 472−475.

(49) Laskowski, R. A.; MacArthur, M. W.; Moss, D. S.; Thornton, J. M. *J. Appl. Crystallogr.* **1993**, *26*, 283−291.

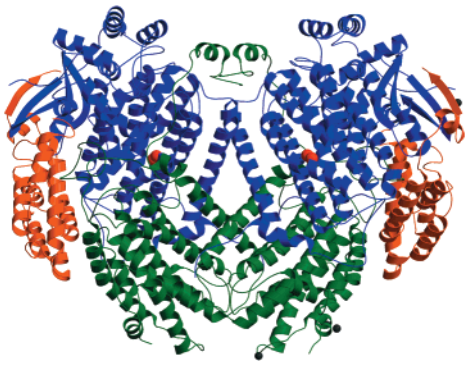

Figure 3. Structure of MMOH from *M. capsulatus* (Bath). The α-subunits are depicted in blue, the β-subunits in green, and the γ-subunits in orange. The iron atoms and calcium atoms appear as red and cyan spheres, respectively. The new β-strand is apparent at the interface of the α- and γ-subunits.

also observed. No electron density was visible for the 16 N-terminal α-subunit amino acids.

Significant electron density in the difference Fourier maps appeared adjacent to surface carboxylate oxygen atoms. Four such features were observed and modeled as hydrated calcium ions, on the basis of the fact that 200 mM $CaCl_2$ was present in the crystallization buffer. All four sites aid in stabilizing the packing of symmetry-related molecules in the crystal. Views of these interactions are presented in Figure S1 (Supporting Information).

Oxidized Active-Site Structure. The active-site structures in the 1.96 Å resolution map of oxidized MMOH are depicted schematically in Figure 4. Since the two halves of the dimer are not related by crystallographic symmetry, there are two independent views of the structure. The two halves of the dimer are very similar, however, with the exception of certain surface residues involved in intermolecular packing interactions, and the geometries of the crystallographically independent diiron centers in these protomers are internally consistent. Glu144 supplies a semi-bridging carboxylate group linking the iron atoms with a tighter bond to Fe1 than to Fe2, as seen in previous structure determinations.[29,32] The Fe−His bonds are all 2.2 Å, but the two imidazole rings are not coplanar. Instead they are canted relative to one another at a dihedral angle of 19°. Residues Glu114, Glu209, and Glu243 all contribute monodentate carboxylate groups. The terminal water molecule bound weakly to Fe1 is held in place by a hydrogen bond to the dangling oxygen atom of Glu114. Electron density consistent with a monodentate bridge proximal to the His residues was modeled as a hydroxide ion. This assignment was the same as that in all previous MMOH structure determinations and is consistent with spectroscopic studies of the enzyme.[40,44] The second oxygen atom of Glu243 forms a tight hydrogen bond to this μ-OH^- group, fixing the carboxylate in place and rendering it unable to form the hydrogen bond to the terminal water molecule on Fe1 observed previously.[29,32] This feature is the first notable difference between the active site in this crystal form and that in crystal form I and in the *M. trichosporium* OB3b MMOH structure.

The second notable difference involves the nature of the bridging species located distal to the two histidines. In the previous structures, this bridging position was occupied either by acetate, μ-OH_2, or μ-OH^-.[27,29,32] The electron density observed in the present structure cannot be adequately explained by any of these chemical entities. We observe a feature that extends outward from the diiron center and bends upward toward

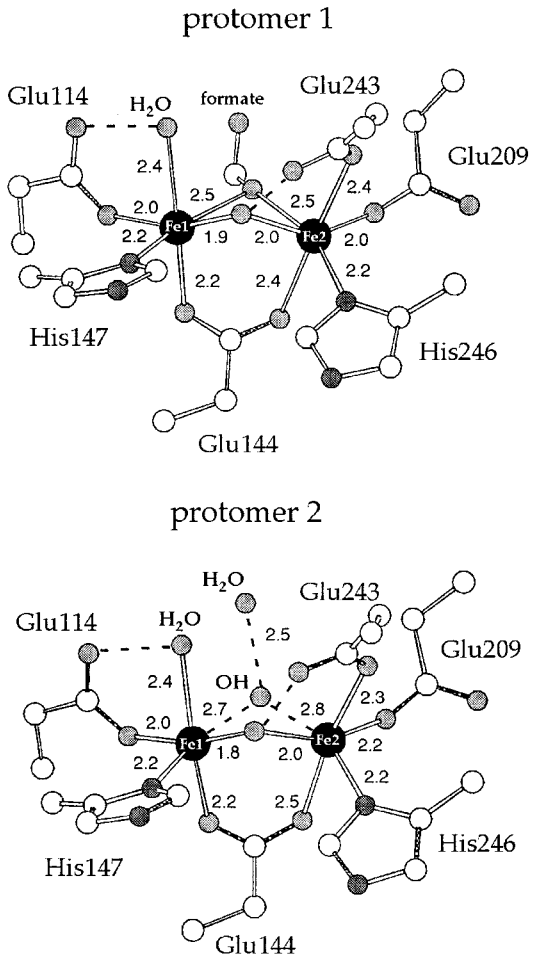

Figure 4. Active-site structure in each protomer of the oxidized MMOH structure. Distances (Å) are as labeled. Dashed lines indicate hydrogen bonding or weakly bonding interactions. The Fe−Fe distances are 3.2 Å in both protomers, and the distance from the Glu243 to the μ-OH moiety is 2.4 and 2.5 Å in protomers **1** and **2**, respectively.

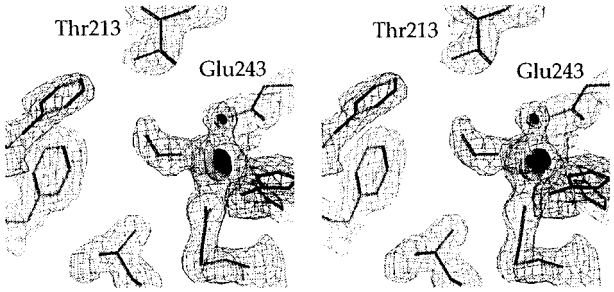

Figure 5. Stereoview of the observed feature of electron density located between the two iron atoms in one protomer of the oxidized structure. Electron density from a simulated annealing omit difference map (3σ contour) surrounds the ligand assigned as formate in the center of the figure, and electron density from a $|2|F_{obs}| - |F_{calc}||$ map (1σ) surrounds the remainder of the structure. The iron atoms are depicted by large black spheres and the terminally bound water molecule by a small black sphere.

the Thr213 residue poised at the top of the active site cavity (Figure 5). A μ-OH^- group and a water molecule, or two water molecules, were introduced to model this electron density in both protomers. In one protomer, their refined positions placed one of them bridging the two iron atoms at distances of 2.7 and 2.8 Å, with the second hydrogen-bonded to the first at a distance of 2.5 Å (Figure 6). The two atoms had *B*-values of 36 and 45 $Å^2$, respectively. The observed distances from the

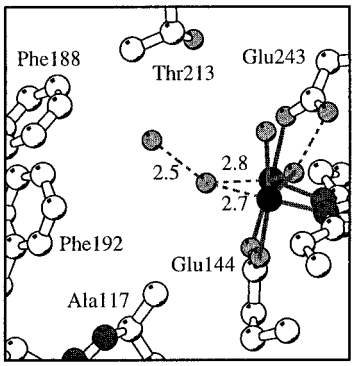

Figure 6. The hydrogen-bonding network involving ordered solvent in the cavity of the oxidized active site in one protomer. The iron atoms are depicted as black spheres, and distances (Å) are as labeled. The distance from the Thr213 hydroxyl group to the closest water molecule is 4.1 Å.

bridging species to the two iron atoms suggested an assignment as a water molecule rather than a second hydroxide, although we do not rule out the possibility of a weakly coordinated $H_3O_2^-$ ion.[50] The hydrogen oxide ion, $H_3O_2^-$, has been demonstrated to be important in the hydrolytic chemistry of classical coordination compounds, and diffraction experiments reveal that this ion is characterized by a very short (~2.5 Å) oxygen−oxygen atom separation.[51−54]

Placing two water molecules into similar positions in the other protomer did not adequately account for all of the observed electron density. Since the assignment of two waters did not here, as above, provide charge neutrality for a diiron(III) active site, we also attempted to model chloride, azide, ethylene glycol, and formate at this position. Refinement of a chloride ion gave *B*-factors >65 Å^2 for the well-defined electron density feature and left residual density, and the linear azide ion did not fit the observed bend; thus, both species were eliminated as possibilities. Ethylene glycol proved to be too large to fit the density but suggested that a bent, three-atom species (excluding hydrogen atoms) could work. Formate was then modeled, and it refined well, giving iron−oxygen bond lengths of 2.4 and 2.5 Å for Fe1 and Fe2, respectively. The *B*-values were in the range 39−48 Å^2, comparable to those of the water molecules in the other protomer. Despite the fact that no formate was added to our crystallization buffers, we consider this assignment to be as likely as the two-water molecule (or $H_3O_2^-$ ion) model in the other protomer. Formate is an intermediate in the biosynthetic pathway of methanotrophic bacteria and could potentially be present in the enzyme as isolated.[55] We stress, however, that we do not as yet have any formal proof that formate can bind to the MMOH active sites.

The hydrogen bond network extending outward from the histidine residues is identical to that observed in previous structures. This network is extensive and provides a well-defined pathway leading to the MMOH surface. The residues involved in it are conserved in all methane monooxygenases, toluene monooxygenases, alkene monooxygenases, and phenol hydroxylases.[56] A similar hydrogen bond network in RNR-R2 is essential for electron transfer in that enzyme.[57] Two other

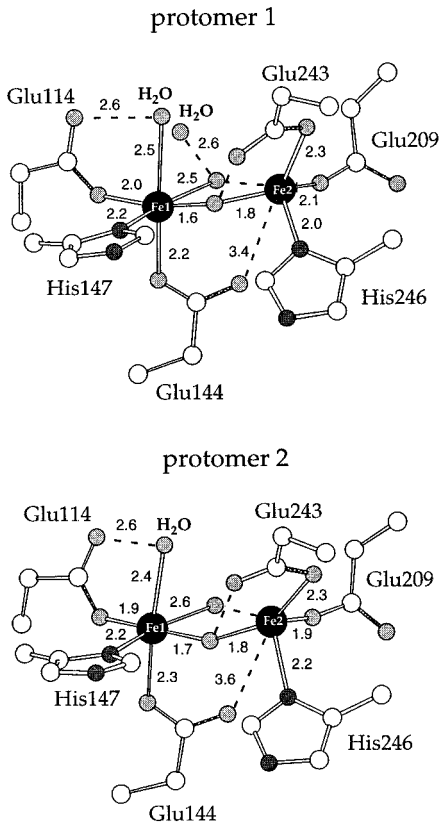

Figure 7. Active-site structure in each protomer of the mixed-valent MMOH structure grown anaerobically. Distances (Å) are as labeled. Dashed lines indicate hydrogen bonding or weakly bonding interactions. The Fe−Fe distances are 3.4 Å in both protomers. The distance from Fe2 to the water molecule distal to the histidine residues is 3.0 and 3.2 Å in protomers **1** and **2**, respectively. Fe2 is roughly tetrahedral with the following angles (averaged over both protomers): μ-OH−Fe2−E243 128°, μ-OH−Fe2−E209 116°, μ-OH−Fe2−H246 94°, E243−Fe2−E209 107°, E243−Fe2 98°, and E209−Fe2−H246 109°.

residues near the active site that have been observed to adopt altered conformations, Leu110 and Asn214, have well-defined electron density.[31,34] Leu110 is in its most common rotameric form, and Asn214 is oriented to point outward from the MMOH surface, away from the active site.

Mixed-Valent Active-Site Structure. Structures of MMOH were determined from crystals grown anaerobically from mixed-valent protein as well as from crystals made mixed-valent by soaking in solutions containing dithionite and mediators. Slight differences were observed for the active sites in mixed-valent MMOH crystals generated by the two methods. The active sites from material grown anaerobically from mixed-valent protein are depicted schematically in Figure 7. Whereas the coordination sphere around Fe1 closely resembles that in the oxidized state, Fe2 is markedly different. The changes are identical in each crystallographically independent protomer. The Fe−Fe separation has increased from 3.2 to 3.4 Å, and Fe2 is now 4-coordinate, with Glu209, Glu243, His246 and the μ-OH$^-$ serving as the four ligands bonded in a tetrahedral fashion. This change is effected by a 1.0 Å movement of Fe2 relative to its position in the oxidized state. Consequently, although Glu144 maintains its same orientation, the distance from its oxygen atom to Fe2 is ~3.5 Å. The dangling oxygen atoms of both Glu144

(50) Ardon, M.; Bino, A. *Struct. Bonding* **1987**, *65*, 1−28.
(51) Abu-Dari, K.; Raymond, K. N.; Freyberg, D. P. *J. Am. Chem. Soc.* **1979**, *101*, 3688−3689.
(52) Abu-Dari, K.; Freyberg, D. P.; Raymond, K. N. *Inorg. Chem.* **1979**, *18*, 2427−2433.
(53) Bino, A.; Gibson, D. *J. Am. Chem. Soc.* **1981**, *103*, 6741−6742.
(54) Bino, A.; Gibson, D. *J. Am. Chem. Soc.* **1982**, *104*, 4383−4388.
(55) Colby, J.; Dalton, H.; Whittenbury, R. *Annu. Rev. Microbiol.* **1979**, *33*, 481−517.
(56) Coufal, D. E.; Blazyk, J. L.; Whittington, D. A.; Wu, W. W.; Rosenzweig, A. C.; Lippard, S. J. *Eur. J. Biochem.* **2000**, *267*, 2174−2185.
(57) Stubbe, J.; Riggs-Gelasco, P. *Trends Biochem. Sci.* **1998**, *23*, 438−443.

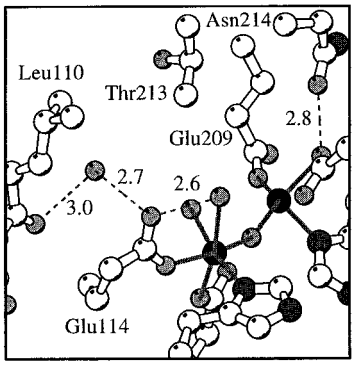

Figure 8. The hydrogen-bonding network involving ordered solvent in the cavity of the mixed-valent active site.

and Glu243 are at hydrogen-bonding distances to the μ-OH$^-$. Additionally, there is no density consistent with a larger, bridging anion, and the water molecule that linked the two iron atoms in protomer **2** is now clearly associated with Fe1, at a distance of 2.5 Å. The distance between this water and Fe2 is now ~3.1 Å. Assignment of this feature as water provides charge neutrality for an Fe(II)Fe(III) active site, assuming that the bridging hydroxide is maintained. The observed bond distances, combined with results from ENDOR spectroscopy and the observed coupling constants derived from EPR experiments, favor the assignment of the bridging species with short Fe−O distances as hydroxide.[40,44] The active-site cavity no longer displays the larger feature of electron density depicted in Figure 5, supporting its assignment as an anion that is displaced in the mixed-valent active site. This overall rearrangement is reminiscent of the changes observed in the diiron center after soaking in 10% DMSO, except that Fe2 was 6-coordinate in that structure due to bidentate chelation by Glu243 and the presence of an additional water molecule.[33]

In addition to the change in Fe2 ligation, new hydrogen-bonding interactions are also observed in these active sites (Figure 8). Electron density consistent with an ordered water molecule appears in the cavity within hydrogen-bonding distance of the backbone carbonyl of Leu110 and the dangling oxygen atom of Glu114. The presence of this water molecule necessitates that Leu110 adopt its most common rotamer, analogous to what is seen in the oxidized structure but in contrast to the results in crystal form I.[31] In addition, owing to the movement of Fe2 and the subsequent adjustment in the Glu243 side chain, the oxygen atom that binds Fe2 is now also within hydrogen-bonding distance of Asn214, which shifts rotamers to point inward toward the active-site cavity. Since Asn214 serves as one of the barriers blocking direct access to the active-site cavity from the protein surface, this change results in altered accessibility to the active site.

In contrast to the changes observed at the active sites of crystals grown anaerobically from mixed-valent protein, oxidized crystals soaked in solutions containing mixed-valent mediators and dithionite exhibit fewer changes by comparison to the oxidized structure. The active sites from these crystals are depicted schematically in Figure 9. Bonds between the iron atoms and Glu209, His246, and the μ-OH$^-$ moiety are maintained. Glu243 appears to shift its position to accommodate the altered position of Fe2, but its movement relative to its position in the oxidized structure is less than in H_{mv} crystallized from solution. The movement of Glu243 results in distances of ~2.8 Å between its oxygen atom and Fe2. Attempts to fix the position of the iron atoms at the 3.4 Å separation observed in the crystals

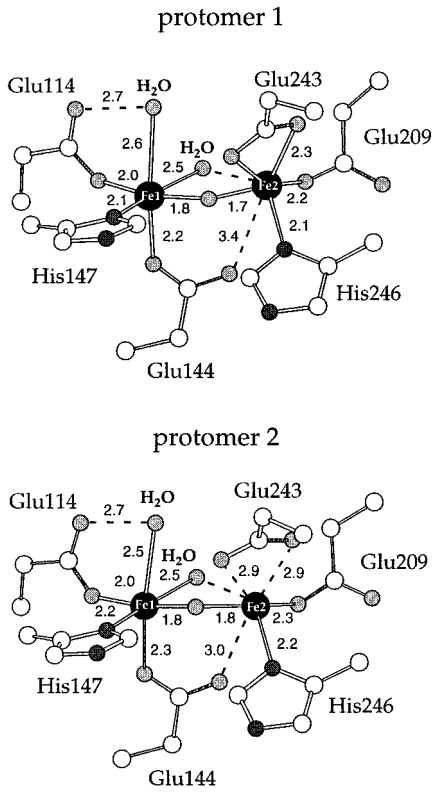

Figure 9. Active-site structure in each protomer of the mixed-valent MMOH structure generated by crystal soaking. Distances (Å) are as labeled. Dashed lines indicate hydrogen bonding or weakly bonding interactions. The Fe−Fe distances are 3.4 and 3.3 Å in protomers **1** and **2**, respectively. In protomer **1**, the second oxygen atom of Glu243 is bonded to Fe2 at a distance of 2.4 Å, making it bidentate chelating. The distances from Fe2 to the water molecule distal to the histidine residues is 3.2 and 2.9 Å in protomers **1** and **2**, respectively.

grown anaerobically resulted in more realistic bonding distances between Fe2 and Glu243 for the first protomer, but residual electron density appeared in the difference Fourier maps between Fe2 and Glu144. A 2.9 Å distance between Glu243 and Fe2 was maintained in the second protomer, with Fe2 being closer to Glu144 than in the first protomer. This result suggests that these crystals contain mixtures of oxidized and mixed-valent hydroxylase, a likely scenario given that, even in solution, it is difficult to convert all of the protein to the mixed-valent state.[19,20]

The active-site cavities in the mixed-valent, soaked structures have electron density consistent with the previously identified water molecule that hydrogen bonds to Glu114 and the carbonyl oxygen atom of Leu110. There is no evidence for additional ordered solvent in the active-site cavity or for the larger feature of density assigned as formate in the oxidized structure. The orientation of Asn214 is the same as in the oxidized structure, protruding out into the solvent, although its density is poorly defined, suggesting that it adopts more than one conformation.

Reduced Active-Site Structure. As with the mixed-valent enzyme, structures were determined for MMOH crystals soaked in solutions of methyl viologen and dithionite to form the diiron(II) center, as well as for crystals grown from diiron(II) protein under anaerobic conditions. Once again, there were differences in the active sites of the protein prepared by the two methods. The active sites from the structure soaked in the reducing solution are depicted schematically in Figure 10. Contrary to what was observed in crystal form I,[32] both active sites in these structures appear to have been reduced. This

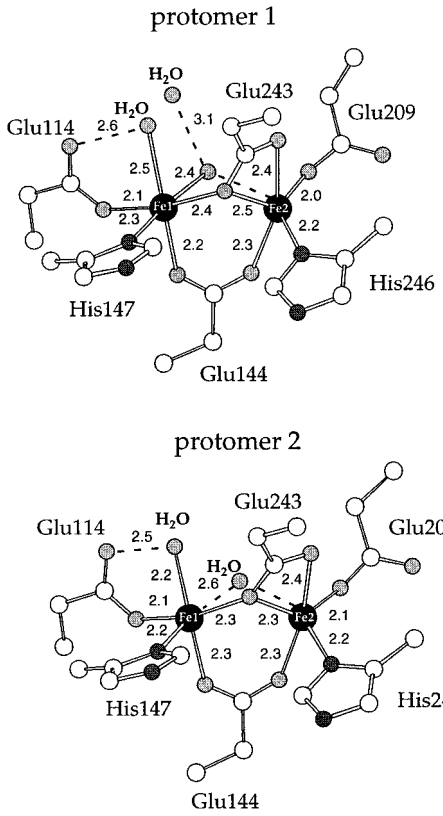

Figure 10. Active-site structure in each protomer of the reduced MMOH structure generated by crystal soaking. Distances (Å) are as labeled. Dashed lines indicate hydrogen bonding or weakly bonding interactions. The Fe−Fe distances are 3.3 Å in each protomer.

structure displays the previously identified carboxylate shift of Glu243 from a monodentate terminal to a bidentate chelating mode to Fe2 and monodentate bridging between the iron atoms.[32] Such an orientation mirrors that observed in the reduced structure of MMOH crystal form I, as well as in the reduced D84E and reduced, azide-soaked F208A/Y122F mutant RNR-R2 structures.[36,37] The μ-OH^- moiety is now gone, and a single water molecule is located in the bridging position distal to the histidines. This ligand composition provides charge neutrality for the diiron(II) center. In contrast to its position in the diiron(III) enzyme, Glu144 bridges the iron atoms more symmetrically in each of the protomers. There are some differences between the active sites in each protomer, however. Two water molecules bind to Fe1 at distances of 2.4 and 2.5 Å in one protomer. This same active site has electron density consistent with two water molecules in the active-site cavity, one hydrogen-bonded to the backbone carbonyl of Leu110 and to one O atom of Glu114, as in the mixed-valent structure, and the second hydrogen-bonded to the first and to the water molecule in the bridging position between the two iron atoms. These water molecules have *B*-values of 44 and 52 $Å^2$, respectively. The active site in the other protomer has only the first water molecule hydrogen-bonded to the Leu110 carbonyl oxygen atom and to Glu114. There is no other identifiable electron density present in the active-site cavity. Also, the water molecule that bridges the two irons is located 2.6 and 2.7 Å away from Fe1 and Fe2, respectively, placing it in the same position as that observed for the bridging water molecule in this protomer in the oxidized structure. At these distances, it is effectively not coordinated, suggesting that it serves as a placeholder, being readily displaced during the approach and reaction of dioxygen to initiate catalysis. The water molecules

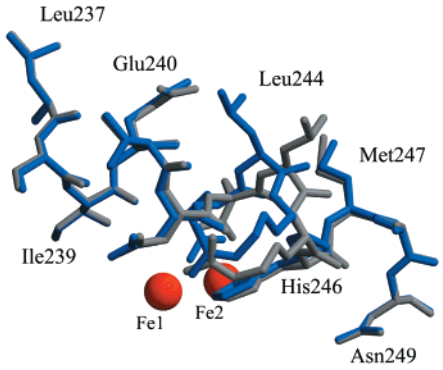

Figure 11. Observed differences in amino acid orientations on helix F in the reduced state (blue) relative to the oxidized state (gray). The iron atoms appear as red spheres.

hydrogen-bonded to the backbone of Leu110 force it to adopt its most common rotamer, identical to what was observed in the oxidized and mixed-valent active sites. In addition, the side chain of Asn214 has rotated inward toward the diiron center in both protomers, with its O atom lining the edge of the active-site cavity, as was noted previously in crystals of form I.[34] Finally, the water molecule that binds to the dangling oxygen atom of Glu209 in the reduced crystals of form I is not observed in this structure.[38]

Shifting Glu243 to a bidentate chelating, monodentate bridging mode between the two iron atoms changes the orientation of the central part of helix F (for nomenclature, see ref 27). In addition to the presence of a π-turn in helix E,[27] all of the MMOH structures show distorted hydrogen bonding in helix F in the vicinity of the dinuclear iron active site. Whereas hydrogen bonds are typically observed between residues *n* and $n + 4$ in an α-helix, in the reduced structure the backbone hydrogen bonds between Leu244−Ala248 and Arg245−Asn249 are broken. This change has the effect of altering the positioning of Leu244 on the solvent-exposed surface of helix F (Figure 11). Arg245 is also shifted, but its guanidinium group maintains an orientation that preserves the His246−Asp143−Arg245 hydrogen-bonding network extending outward from the active site. This altered conformation of the F helix is not observed in the oxidized or mixed-valent structures.

The structure of the active sites in the crystals grown from diiron(II) protein under anaerobic conditions is markedly different from those in the crystals soaked in reductants. These active sites appear to have lost Fe2, leaving only a single iron atom in the active site (Figure 12). This observation suggests that the iron atoms are more labile in the Fe(II) state and that Fe1 binds more tightly than Fe2. The preferential loss of Fe2 is consistent with it being more mobile, as reflected by its higher average *B*-values relative to those of Fe1 and by its altered location in the DMSO-soaked MMOH crystals.[32,33] This result is in direct contrast to the relative lability of the iron atoms in *E. coli* and mouse RNR-R2, in which Fe2 binds more tightly.[58,59] The absence of Fe2 results in an altered conformation of Glu144, causing the carboxylate moiety to rotate slightly and to become a monodentate terminal ligand to Fe1. His147 maintains its orientation, but Glu114 alters its conformation slightly in one protomer. The terminal water molecule is no longer observed on Fe1. This arrangement results in only three observable ligands

(58) Kauppi, B.; Nielsen, B. B.; Ramaswamy, S.; Kjoller Larsen, I.; Thelander, M.; Thelander, L.; Eklund, H. *J. Mol. Biol.* **1996**, *262*, 706−720.

(59) Bollinger, J. M., Jr.; Chen, S.; Parkin, S. E.; Mangravite, L. M.; Ley, B. A.; Edmondson, D. E.; Huynh, B. H. *J. Am. Chem. Soc.* **1997**, *119*, 5976−5977.

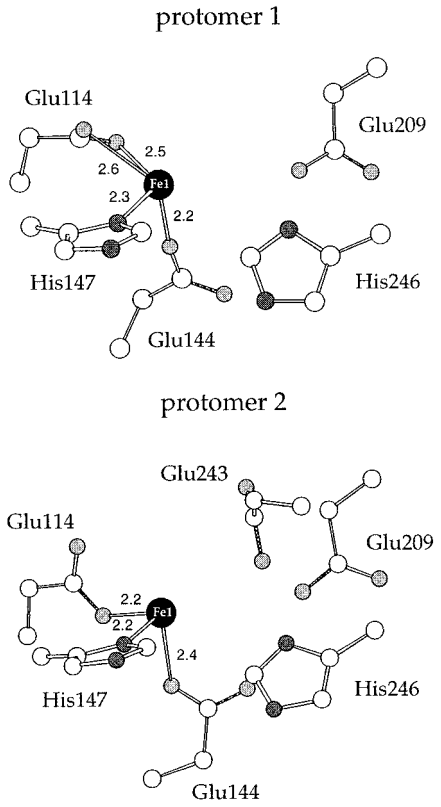

Figure 12. Active-site structure in each protomer of the reduced MMOH structure grown anaerobically. Distances (Å) are as labeled. The incomplete models reflect the disorder observed in these active sites; only components with well-defined electron density are depicted.

to Fe1, which is probably a reflection of disorder among terminal water ligands, although the poorer quality diffraction data for this variant diminishes our ability to discern solvent in the electron density maps. Residual electron density does exist in the difference Fourier maps at the Fe2 site. A single atom placed in the center of this feature is located 2.5 Å from Fe1 and <2.2 Å from the Nδ atom of His246 and one oxygen atom of Glu209. The closest oxygen atom of Glu243 is positioned 2.7 Å from this location in one active site, but in the other there is no electron density for Glu243 beyond the β carbon, suggesting that the carboxylate side chain samples a range of orientations. The Glu209 and His246 locations with respect to the feature of difference Fourier electron density suggests that the Fe2 site is partially occupied. Refinement of the Fe2 occupancy with a *B*-factor fixed at the value of the Fe1 site results in an average occupancy of 0.66. Refinement of occupancies at both iron sites, using the *B*-values from the Fe sites in the reduced, soaked crystal yields average occupancies of 0.71 and 0.48 for the Fe1 and Fe2 sites, respectively.

The well-defined electron density for Glu209 and His246 suggests that they maintain their same orientations even in the Fe-free sites, assisted by hydrogen bonds between Glu209 and Gln140 and between His246 and Asp143. One Fe(II) ion would account for only two of four potentially negatively charged carboxylates at the active site. Protonation and hydrogen bonding of the free ligands would help to neutralize these buried charged residues. Similar hydrogen-bonding interactions have been observed in the structure of apo-RNR-R2.[60] In addition, a partially occupied single iron site occurs in mouse RNR-R2, although the composition of this site at pH 4.7 may not reflect its true nature at physiological pH.[58] Without Fe2 present, Asn214 now adopts a conformation pointing outward, away from the active site, analogous to that found in the oxidized structure. Although this structure provides a clear view of neither the reduced nor the apo form of the enzyme, it indicates an increased lability of the ferrous ions in MMOH.

Effect of pH on Active-Site Structure. MMOH crystals do not grow under our established conditions at pH 6.2, and only tiny crystallites form at pH 8.5. Consequently, the effect of pH on the MMOH structure was investigated by soaking oxidized crystals in solutions containing either 0.1 M PIPES, pH 6.2, or 0.1 M Tris, pH 8.5, in place of the 50 mM MOPS, pH 7.0, that is normally present. Soaking at pH values much above or below these values resulted in destruction of the crystals. Large differences in active-site structures were not expected since the only groups expected to have pK_a values in the range examined were histidine and possibly metal-bound solvent molecules. The active-site structure at pH 6.2 matches that of the oxidized structure at pH 7.0 almost exactly (Figure S2). The same Fe−Fe separation, Fe-ligand distances, and bridging electron density features are observed. The bridging electron density distal to the histidine residues is fit better by two solvent molecules in one protomer, and by a formate anion in the other protomer, analogous to the pH 7.0 structure. The rotamers observed for Leu110 and Asn214 are also identical to those observed at pH 7.0.

The pH 8.5 structure was determined at lower resolution than either the pH 7.0 or pH 6.2 structures, making exact comparison of the relative Fe−Fe separations and Fe-ligand bond lengths more difficult. The general features of the active site at pH 8.5 resemble those at pH 7.0, however (Figure S3). The only differences are a lengthening of the distance between the iron ions and Glu144, and the apparent absence of the terminal water molecule on Fe1 in one of the protomers. Electron density in the active-site cavities is very poorly defined, but formate can be built into the cavity of one protomer, by analogy to the pH 6.2 and 7.0 structures, and it refines to reasonable positions and *B*-factors. No electron density is present in the active-site cavity in the second protomer, nor are additional differences observed in more remote regions of the protein. Intermolecular contacts in the crystals are undisturbed.

Statistical Comparison of Active-Site Structures. Seven independent structures of the dimeric MMOH protein are reported here, giving 14 independent views of the dinuclear iron active site. Several of these structures have similar active-site geometries, but superimposing the oxidized pH 7.0 structure, the reduced, soaked structure, and the anaerobically grown mixed-valent structure demonstrates the range of possible motions (Figure 13). It is apparent that ligands donated by helices E and F sweep out a much larger space than the amino acids located on the B and C helices. This behavior is also reflected by higher average *B*-factors for Fe2, Glu209, His246 and Glu243, relative to those in the rest of the active site. The *B*-values for these residues, averaged over all of the structures presented here, are 43−50 Å^2, in contrast to the average *B*-values of 26−33 Å^2 for Glu114, Glu144, and His147, which are on the order of the average *B*-values for all atoms in the structures (see Table 2). Outside of the immediate vicinity of the diiron center, the MMOH structure displays no changes related to the redox states of the iron atoms. The α-subunits from the structures reported can be superimposed with rmsd values of ≤0.16 Å.

Discussion

Novel Findings of this Study. The series of high-resolution X-ray crystal structures of MMOH presented here provides an

(60) Aberg, A.; Nordlund, P.; Eklund, H. *Nature* **1993**, *361*, 276−278.

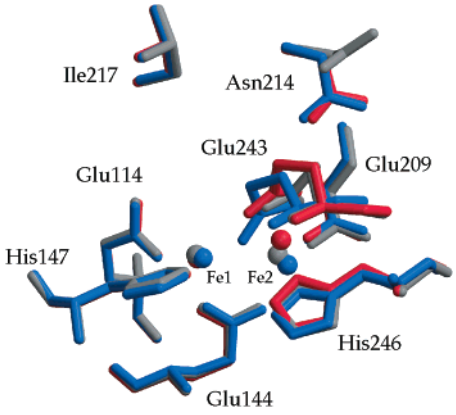

Figure 13. Superposition of the oxidized (gray), mixed-valent (red), and reduced (blue) diiron sites demonstrating the range of observed motions. Fe1 maintains the same position in all structures, while Fe2 moves significantly.

unprecedented level of structural detail with which to examine the first and second coordination spheres of the dinuclear iron active site. The results provide the first view of the active site in the mixed-valent oxidation state, revealing a novel geometry of the diiron center containing one 6-coordinate and one 4-coordinate iron atom. In this arrangement, Asn214 adopts a rotamer pointing inward toward the diiron center such that it can hydrogen bond directly to the dangling oxygen atom of Glu243. This conformation has the added affect of altering the surface of MMOH in the vicinity of the active site. In the diiron(II) structure obtained from crystal-soaking experiments, Asn214 adopts the analogous inward-pointing rotamer, but the conformation of Glu243 is such that the two do not form a hydrogen bond. The altered conformation of Glu243 in this structure, which was observed previously,[32] also affects the conformation of Leu244 and Arg245 and results in a third surface arrangement for MMOH in the vicinity of the active site. These variable surfaces may have important implications for the interactions of MMOH with the MMOB and MMOR components, and for substrate and product access to the hydrophobic active-site cavity, cavity 1. Crystals of MMOH grown from the diiron(II) enzyme were also produced, but they were depleted in iron content at the Fe2 position. This unexpected result indicates increased lability of the Fe(II) relative to Fe(III) ions and indicates that the iron atom at the Fe1 position is more tightly bound. In the diiron(III) enzyme, the active site has a geometry very similar to those observed in previous X-ray studies, but electron density bridging the two iron atoms in cavity 1 is assigned either as a formate or an $H_3O_2^-$ anion. Such an assignment both accounts for its shape and renders the site charge neutral. Comparison of the diiron(III) enzyme structures at pH values of 6.2, 7.0, and 8.5 did not reveal any significant differences. Finally, the high-quality electron density maps allowed the tracing of additional amino acids at the termini of certain protomers and resulted in the identification of an additional β-strand in the γ-subunit that extends the β-sheet formed by residues in the adjacent α-subunit.

Nature of the Bridging Ligand in Cavity 1 at the Active Site. In view of the extended electron density present at this position in the oxidized structure (Figure 5) and to obtain charge neutrality in the diiron(III) active site, we propose that formate and $H_3O_2^-$ can serve as anionic ligands to the iron atoms in MMOH. To the best of our knowledge, the $H_3O_2^-$ anion has not previously been identified in a metalloprotein. Its presence may have been overlooked, however, a possible example being the bridging ligand linking the cobalt ions in methionine aminopeptidase.[61] Previous X-ray studies have indicated the presence of acetate,[27] hydroxide,[29] and methoxide[62] as bridging ligands protruding into active-site cavity 1 of H_{ox}. Collectively, these results suggest that a range of anions can be accommodated, provided that they are of the appropriate size to fit into the cavity. Within the cell, methoxide, hydroxide, $H_3O_2^-$, and formate are the most likely such ligands. Under favorable growth conditions, however, the diiron(III) enzyme is rapidly converted to the diiron(II) state during turnover, since methane oxidation provides the sole source of carbon and energy in obligate methanotrophic bacteria such as *M. capsulatus* (Bath).[55] If formate is the ligand observed in the present structures, a feedback inhibition mechanism is suggested since formate is produced by methanotrophic bacteria at a later, energy-producing step in their metabolic pathway.[55]

Relation to Previous Spectroscopic Work. The observed differences in the MMOH active-site structures presented in this work correlate nicely with spectroscopic studies of the enzyme from both the *M. capsulatus* (Bath) and *M. trichosporium* OB3b systems. Electron nuclear double resonance (ENDOR) spectroscopy has been used to probe the binding of small molecules to the active site. Early work demonstrates the presence of a hydroxide bridge in mixed-valent MMOH and outlines a model for DMSO binding to the Fe(III) ion in the mixed-valent state.[44,63] Subsequent experiments show that DMSO, methanol, and water can simultaneously bind to the mixed-valent active site, with water and methanol coordinated to the Fe(II) ion.[41] In the structure depicted in Figure 7, the μ-OH^- and the amino acid ligands to Fe2 do not permit the binding of more than one exogenous ligand to the metal ion. Consequently, one can envision DMSO coordinating to the open position on Fe2 and methanol binding at the site occupied by one of two water molecules on Fe1. The other water molecule on Fe1, presumably the one hydrogen-bonded to Glu114, would remain, thereby providing a model that satisfies the ENDOR results. Since the estimated error in the crystallographically determined bond lengths is not sufficient to distinguish oxidation states, however, we cannot definitively assign the charges of the individual iron ions. Finally, EXAFS measurements of the mixed-valent enzyme indicate an Fe−Fe separation of 3.4 Å, which matches that observed in crystals grown from H_{mv}.[40]

As a complement to ENDOR studies, MMOH was investigated by EPR spectroscopy of oxidized samples cryoreduced by one electron at 77 K to yield the mixed-valent oxidation state having the geometry the diiron(III) enzyme.[22] The results indicate that methanol and phenol can bind to the diiron(III) center. Although DMSO bound to the diiron center in the mixed-valent state, it had no observable effect on the EPR properties of the diiron(III) site. When protein B was added to the samples, however, DMSO was again able to bind to the diiron(III) site. These results indicate a differential accessibility of the dinuclear iron center in the two oxidation states. Comparing the oxidized and mixed-valent structures presented in this work reveals differences in the positions of Fe2, Glu243, and Asn214 between the two. This structural rearrangement effects a change at the protein surface on the solvent accessible side of helix F. The rotation of Asn214 inward to hydrogen bond to Glu243 opens access to the active site. This change must somehow be mitigated by MMOB binding, which restricts, but does not

(61) Lowther, W. T.; Orville, A. M.; Madden, D. T.; Lim, S.; Rich, D. H.; Matthews, B. W. *Biochemistry* **1999**, *38*, 7678−7688.
(62) Whittington, D. A.; Sazinsky, M. H.; Lippard, S. J. *J. Am. Chem. Soc.* **2001**, In press.
(63) DeRose, V. J.; Liu, K. E.; Lippard, S. J.; Hoffman, B. M. *J. Am. Chem. Soc.* **1996**, *118*, 121−134.

block, the pathway to the active site. Although a complete understanding of the changes in MMOH upon MMOB binding is not yet possible, the results of circular dichroism and magnetic circular dichroism spectroscopy indicate that MMOB binding causes a change at only one iron site in MMOH.[23,64] This iron atom was suggested to be Fe2, an assignment that is logical in view of the structural results presented here demonstrating that the coordination environment around Fe2 can move significantly while that around Fe1 stays fixed (Figure 13).

Implications for Component Interactions. Thermodynamic models for MMOB binding to the different redox states of MMOH suggest that it has the strongest affinity for MMOH in the oxidized state.[19,25] A comparison of the MMOH structures in the three redox states indicates that all of the differences in surface features are centered on the same face of helix F. Asn214 and Glu243 make up part of this surface and both residues adopt altered conformations, depending upon oxidation state. Moreover, the carboxylate shift in the reduced enzyme distorts the α-helical hydrogen bonding that alters the orientations of Leu244 and Glu240 (Figure 11). Although we cannot rule out the possibility that longer-range changes may also occur that are blocked by crystal packing, it seems most reasonable to concludethat alterations in this surface affect protein B binding and vice versa. This conclusion supports previous proposals that protein B binds to the canyon region of MMOH and exerts its effects, at least in part, by altering residues on helices E and F.[23,27,56] The proposal is also consistent with the observed cross-linking of protein B to the α-subunit of MMOH.[65] Since the proposed interaction is so localized, the cluster of Asn214, Leu244, and Glu240 makes an attractive target for site-directed mutagenesis aimed at probing the MMOH−MMOB interaction. Asn214 is conserved in toluene monooxygenase, phenol hydroxylase, and alkene monooxygenase systems, all of which utilize hydroxylase components under the control of similar, small regulatory proteins.[56]

MMOB increases the rates of formation and decay of intermediates in the sMMO cycle and controls rates of electron transfer to the diiron site.[21,26] Since EXAFS spectroscopy indicates that protein B binding does not change the primary coordination sphere of the iron atoms, these effects must be exerted through alternative hydrogen-bonding and/or side chain packing arrangements.[66,67] In the reduced enzyme, Asn214 is oriented to point inward toward the active site, but it cannot hydrogen bond to the carboxylate-shifted Glu243 residue. Although no ordered solvent binds to Asn214 in the reduced structures, it has the potential to contribute to ordered hydrogen bonding in the active-site cavity. Since MMOB could very easily affect the Asn214 orientation, the rate increases may correspond to what is ordered, or disordered, in the cavity. Studies with the *M. trichosporium* OB3b enzyme indicate that a single proton is required in the transition state for the formations of both H_{peroxo} and Q, the two spectroscopically observable intermediates in the sMMO catalytic cycle.[39] The measured pK_a of both transitions is 7.6, making an Fe-bound solvent molecule an attractive source for these protons. Recent density functional theory calculations on MMOH indicate that one water molecule may indeed stay bound to Fe1 through the catalytic cycle.[38] If additional ordered hydrogen-bonding partners are not available in the active site during catalysis, the protons from this water molecule are free to interact with O_2-derived oxygen atoms in the catalytic intermediates. MMOB has also been suggested previously to alter hydrogen bonding in the active site to affect the conformation of Leu110.[31] The results presented here demonstrate that there is indeed an ordered water molecule that hydrogen bonds to the backbone carbonyl of Leu110, forcing it to adopt a certain rotamer. If MMOB binding were to disrupt ordered solvent in the active site, the Leu110 side chain would be free to adopt either of its two preferred rotameric states, facilitating its proposed role in gating access to the active-site cavity 1 from the adjacent hydrophobic cavity 2.

The effect of MMOB on electron transfer may also be exerted by changes in the hydrogen-bonding patterns in MMOH. The crystal structures of reduced MMOH show an altered orientation in helix F that causes a change in the location of the Arg245 side chain. If MMOB were to bind and exert an effect on this helix, movement of Arg245 could provide a direct link to the extensive hydrogen bond network that extends from one side of the active site. This network contains nine residues, including the two His ligands to the iron, that are absolutely conserved in the family of toluene monooxygenase, phenol hydroxylase, and alkene monooxygenase enzymes, as well as methane monooxygenases.[56] RNR-R2 and Δ9-ACP also exhibit hydrogen-bonding networks at analogous locations, and the one in RNR-R2 is important for electron transfer.[57] In MMOH, this network is the only one of its kind in the vicinity of the active site and it extends to residues Tyr67 and Lys74, which are located near the protein surface. By analogy to RNR-R2, these conserved amino acids may potentially play a role in electron transfer to the diiron center. The distance from the surface of this network to the diiron center is 10−11 Å, which is less than the 14 Å distance suggested to be the upper limit on the separation between cofactors in redox active enzymes.[68] This hypothesis is best tested with the use of site-directed mutants of the hydrogen-bonded network of MMOH.

Relation to Other Diiron Enzymes. Given the wealth of structural and spectroscopic information on MMOH and the closely related RNR-R2 and Δ9-ACP enzymes, some of the similarities and differences between them can begin to be assessed. Whereas the protein-derived ligands are nearly the same in each enzyme, the surrounding protein residues are not. This dissimilarity has implications for the control of the catalytic process, since each system has unique substrates and redox-active partner proteins with which they must interact. The activity of MMOH is intimately associated with the effects of MMOB. Significant experimental evidence exists to indicate that MMOB binds to MMOH and causes changes in the local environment around the iron center that perturb Fe2. In MMOH, Fe2 is the more labile ion and undergoes a range of motions depending upon redox state. RNR-R2 and Δ9-ACP are not subject to regulation by a protein analogous to MMOB. The helices in these proteins corresponding to helix F in MMOH display less distorted hydrogen-bonding patterns and are likely to be less sensitive to conformational variation than the analogous regions in MMOH. Consistent with this observation is the fact that Fe2 is less labile than Fe1 in the RNR-R2 systems.[58,59] In contrast to the MMOH and RNR-R2 systems, the active site of Δ9-ACP undergoes a dramatic change upon addition of substrate.[69] This change places the diiron(II) center in a geometry different from that of the other two systems. The

(64) Pulver, S.; Froland, W. A.; Fox, B. G.; Lipscomb, J. D.; Solomon, E. I. *J. Am. Chem. Soc.* **1993**, *115*, 12409−12422.
(65) Fox, B. G.; Liu, Y.; Dege, J. E.; Lipscomb, J. D. *J. Biol. Chem.* **1991**, *266*, 540−550.
(66) DeWitt, J. G.; Rosenzweig, A. C.; Salifoglou, A.; Hedman, B.; Lippard, S. J.; Hodgson, K. O. *Inorg. Chem.* **1995**, *34*, 2505−2515.
(67) Shu, L.; Liu, Y.; Lipscomb, J. D.; Que, L., Jr. *J. Biol. Inorg. Chem.* **1996**, *1*, 297−304.
(68) Page, C. C.; Moser, C. C.; Chen, X. X.; Dutton, P. L. *Nature* **1999**, *402*, 47−52.
(69) Yang, Y.-S.; Broadwater, J. A.; Pulver, S. C.; Fox, B. G.; Solomon, E. I. *J. Am. Chem. Soc.* **1999**, *121*, 2770−2783.

methane and dioxygen substrates of MMOH and RNR-R2 do not effect such changes.

Despite the differences in regulation between these enzymes, however, their similarities with regard to dioxygen activation are striking. All three form similar diiron(III) peroxide intermediates, MMOH and RNR-R2 utilize intermediates containing high-valent Fe(IV), and RNR-R2 will even perform oxidation chemistry, similar to that of MMOH, if the right mutations are made.[70−72] Many questions remain, however, the answers to which will no doubt reveal more effects of protein dynamics and the role of protein−protein interactions. A more thorough understanding of MMOH catalysis, from which may come better understanding of its relation to other diiron enzymes, awaits the more detailed understanding of the molecular effects of interactions between the three protein components of the MMO system.

(70) Ormö, M.; deMaré, F.; Regnström, K.; Aberg, A.; Sahlin, M.; Ling, J.; Leohr, T. M.; Sanders-Loehr, J.; Sjöberg, B.-M. *J. Biol. Chem.* **1992**, *267*, 8711−8714.

(71) Aberg, A.; Ormö, M.; Nordlund, P.; Sjöberg, B.-M. *Biochemistry* **1993**, *32*, 9845−9850.

(72) Logan, D. T.; deMaré, F.; Persson, B. O.; Slaby, A.; Sjöberg, B.-M.; Nordlund, P. *Biochemistry* **1998**, *37*, 10798−10807.

Acknowledgment. This work was supported by a Grant from the National Institutes of Health (GM32134 to S.J.L.), and D.A.W. was partially supported by a Biotechnology Training Grant from the NIH. The work is based in part upon research conducted at the Stanford Synchrotron Radiation Laboratory (SSRL), which is funded by the Department of Energy (BES, BER) and the National Institutes of Health (NCRR, NIGMS). Use of the Argonne National Laboratory Structural Biology Center (SBC) beamline 19-ID at the Advanced Photon Source was supported by the U.S. Department of Energy, Office of Biological and Environmental Research under Contract No. W-31-109-ENG-38. We gratefully acknowledge the help of A. Cohen at SSRL, and F. J. Rotella and N. E. C. Duke at the SBC. We thank D. A. Kopp, U.-M. Ohndorf, M. H. Sazinsky, B. Spingler, and A. Yarnell for assistance with data collection.

Supporting Information Available: Figures depicting the structures of the MMOH active sites at pH 6.2 and pH 8.5, and the location of bound Ca^{2+} ions on MMOH (PDF). This material is available free of charge via the Internet at http://pubs.acs.org.

JA003240N